

Aerosol speciation and mass prediction from toluene oxidation under high NO_x conditions

Janya L. Kelly^{a,b,*}, Diane V. Michelangeli^{a,1}, Paul A. Makar^{a,b}, Donald R. Hastie^c, Michael Mozurkewich^c, Janeen Auld^c

^a Department of Earth and Space Science and Engineering, York University, 4700 Keele Street, Toronto, Ontario, Canada M3J 1P3

^b Air Quality Modelling and Integration Section, Air Quality Research Division, Atmospheric Science and Technology Directorate, Science & Technology Branch Environment Canada, 4905 Dufferin Street, Toronto, Canada M3H 5T4

^c Department of Chemistry, York University, 4700 Keele Street, Toronto, Ontario, Canada M3J 1P3

ARTICLE INFO

ABSTRACT

A kinetically based gas-particle partitioning box model is used to highlight the importance of parameter representation in the prediction of secondary organic aerosol (SOA) formation following the photo-oxidation of toluene. The model is initialized using experimental data from York University's indoor smog chamber and provides a prediction of the total aerosol yield and speciation. A series of model sensitivity experiments were performed to study the aerosol speciation and mass prediction under high NO_x conditions (VOC/NO_x = 0.2). Sensitivity experiments indicate vapour pressure estimation to be a large area of weakness in predicting aerosol mass, creating an average total error range of 70 μg m⁻³ (range of 5–145 μg m⁻³), using two different estimation methods. Aerosol speciation proved relatively insensitive to changes in vapour pressure. One species, 3-methyl-6-nitro-catechol, dominated the aerosol phase regardless of the vapour pressure parameterization used and comprised 73–88% of the aerosol by mass. The dominance is associated with the large concentration of 3-methyl-6-nitro-catechol in the gas-phase. The high NO_x initial conditions of this study suggests that the predominance of 3-methyl-6-nitro-catechol likely results from the cresol-forming branch in the Master Chemical Mechanism taking a significant role in secondary organic aerosol formation under high NO_x conditions. Further research into the yields and speciation leading to this reaction product is recommended.

Crown Copyright © 2009 Published by Elsevier Ltd. All rights reserved.

Keywords:

Toluene oxidation
Secondary organic aerosol
Aerosol modelling
Vapour pressure estimation

1. Introduction

Organic material contributes ~20–50% to the total fine aerosol mass at continental mid-latitudes and up to 90% in tropical forested areas (Kanakidou et al., 2005). The organic component of an ambient aerosol contains a mixture of hundreds of organic compounds, including oxidation products of aromatic hydrocarbons, an important class of organic compounds found in fossil fuel emissions and urban air accounting for 40% of the non-methane hydrocarbons (Seinfeld and Pandis, 1998). Of the 32 most prevalent non-methane hydrocarbons observed in urban air, seven are aromatic. Toluene accounts for approximately 6% of the observed non-methane hydrocarbon, making it the most abundant aromatic compound in urban air (Jeffries, 1995).

Secondary organic aerosols (SOAs) are formed from the gas-particle partitioning of semi-volatile organic gases resulting from the atmospheric oxidation of organic compounds and are an important contribution to the atmospheric fine particulate burden, especially during severe urban smog episodes (Turpin and Huntzicker, 1995).

A series of chamber studies have been performed using toluene as the reactive hydrocarbon (Gery et al., 1985; Izumi and Fukuyama, 1990; Forstner et al., 1997; Odum et al., 1997; Kleindienst et al., 1999; Hurley et al., 2001; Jang and Kamens, 2001; Barbu, 2003; Sato et al., 2004, 2007; Johnson et al., 2004; Huang et al., 2006; Hao et al., 2007; Hu and Kamens, 2007; Hu et al., 2007; Ng et al., 2007; Hildebrandt et al., 2009). The formation of SOA has been studied theoretically by Pankow (1994a,b), Kamens et al. (1999), Jang and Kamens (2001), Jiang (2003), Sato et al. (2004), Stroud et al. (2004), Barsanti and Pankow (2005a,b, 2006), Donahue et al. (2005), Presto et al. (2005), Song et al. (2005), Donahue et al. (2006), Jang et al. (2006) and Xia et al. (2008). These studies examine not only how the gas-phase species enter into the aerosol phase, but also examine how surrounding conditions influence the aerosol yield,

* Corresponding author at: Air Quality Research Division, Environment Canada, 4905 Dufferin Street, Toronto, Ontario, Canada M3H 5T4. Tel.: +1 416 514 2658; fax: +1 416 739 4288.

E-mail address: janya.kelly@ec.gc.ca (J.L. Kelly).

¹ Deceased August 30, 2007.

and explore possible reactions and physical descriptions of the aerosol formation process itself.

This study aims to understand the behaviour of the predicted SOA concentration and detailed SOA speciation under very high NO_x conditions. The box model used in this study has the ability to individually track species in the gas and aerosol phase, as well as their partitioning between the phases, providing predictions of aerosol speciation. The model incorporates a detailed mechanism for toluene oxidation (discussed below) and uses a kinetically based gas-particle partitioning approach; it is initialized from experimental smog chamber data. While it is recognized that there is uncertainty associated with many of the prediction methods used in SOA modelling, few choose to present the range of possible modelled values in their results. This study looks at the implications of vapour pressure on proposed aerosol speciation and yield, including a brief study on the impact of vapour pressure estimation method choice. To achieve this, a series of sensitivity tests were performed using the model to simulate SOA formation.

2. Experimental description

The data used in this evaluation were obtained from HO radical initiated toluene oxidation studies performed in an 8 m^3 Teflon-walled indoor smog chamber at York University by Barbu (2003). A detailed description of the smog chamber can be found in Stroud et al. (2004) and in Kelly (2007). Experiments were performed in the cylindrically shaped York University smog chamber, with Teflon coated aluminum endplates and transparent Teflon walls. It is approximately 8 m^3 in volume, can be irradiated by up to 24 ultraviolet lights (Philips F40BL, 40 W), and has an internal electric fan to enhance mixing. The chamber was flushed with clean air before each experiment for approximately 36 h. These experiments were run using initial conditions of ammonium sulphate ($(\text{NH}_4)_2\text{SO}_4$) seed particles, nitric oxide (NO), and isopropyl nitrite (IPN, $(\text{CH}_3)_2\text{CHONO}$) as the source of the hydroxyl radical. The gas-phase reactants were introduced to the chamber with an approximate relative mixing ratio of 1/5/10 ppmv for the three components (toluene/NO/IPN), respectively (actual mixing ratios shown in Table 1). These conditions were used to limit the build up of ozone in the system, allowing further reaction of products by ozone to be ignored. Limiting the formation of ozone also limits the formation of NO_3 radicals in the system, potentially impacting the aerosol species formed. These conditions are at the high end of NO/toluene ratios used in experiments reported by other groups. Reactants and seed particles were introduced into the dark chamber and allowed to mix for 1 h, during which time gas and particle phase measurements were taken. The relative humidity inside the chamber was less than 10% for all experimental runs. After one hour the lights were turned on, initiating HO production in the chamber. For the duration of each experiment (1–4 h) gas and particle phase measurements were taken every 5 min. The chamber was run with an average inside temperature of 304 K and a relative humidity of 6%. All the concentrations and the particle mass were corrected for

Table 1
Initial conditions for chamber experiments conducted by Barbu (2003).

Experiment date	Toluene (ppmv)	NO (ppmv)	IPN (ppmv)	Seed mass ($\mu\text{g m}^{-3}$)	Geometric mean (nm)	σ_g
2001-1	0.73	2.81	7.25	6.92	49.24	1.60
2001-2	0.15	1.03	1.52	7.07	50.05	1.61
2001-3	0.24	1.36	2.40	6.64	49.85	1.60
2001-4	0.73	2.37	7.30	6.69	48.46	1.62
2001-5	0.38	1.78	3.75	10.11	51.63	1.61
2001-6	0.38	1.87	3.82	7.82	48.64	1.61

the dilution induced by maintaining the pressure and volume of gas in the chamber by replacing the air sampled by the monitors with clean air.

The organic aerosol mass concentration is derived from the size distributions, assuming a particle density of 1.4 g cm^{-3} (Stroud et al., 2004; Kelly, 2007), in accord with measurements by Pitz et al. (2003).

Six experiments for seeded toluene oxidation were selected from Barbu (2003), based on data completeness. Fig. 1 shows the final organic particulate mass yield plotted as a function of organic particle mass produced for all experiments. The uncertainty in the organic mass produced is estimated as ranging from 10 to 20% (Barbu, 2003). The initial and final values for all six experiments are listed in Tables 1 and 2. Two experiments are selected and highlighted for discussion and analysis here (2001-3 and 2001-6).

Comparison to other toluene oxidation studies show the experimental aerosol mass is higher than expected, given the amount of NO present in the chamber. Ng et al. (2007) have observed that high aerosol yields seem to be associated with high oxidation rates. More published information is needed from other oxidation experiments (such as hydrocarbon decay, NO_x data and aerosol mass evolution) to provide a proper comparison and verify the potential for differences in oxidation rate as a cause for inter-chamber SOA formation differences. A box model such as that presented below could also be useful in testing this hypothesis, provided the necessary information mentioned above is available.

3. Model description

A box model is used to represent the chemistry and micro-physics associated with the gas-particle partitioning in the smog chamber. A detailed gas-phase chemical mechanism and kinetic gas-particle partitioning are used to simulate the secondary organic aerosol (SOA) formation and to examine the accuracy of the partitioning process representation.

3.1. Chemical mechanism

The model employs the near-explicit toluene oxidation scheme, a subset of the Master Chemical Mechanism (MCM) version 3.1, developed at the University of Leeds (Bloss et al., 2005a,b). It has been noted that there are a number of known shortcomings in the

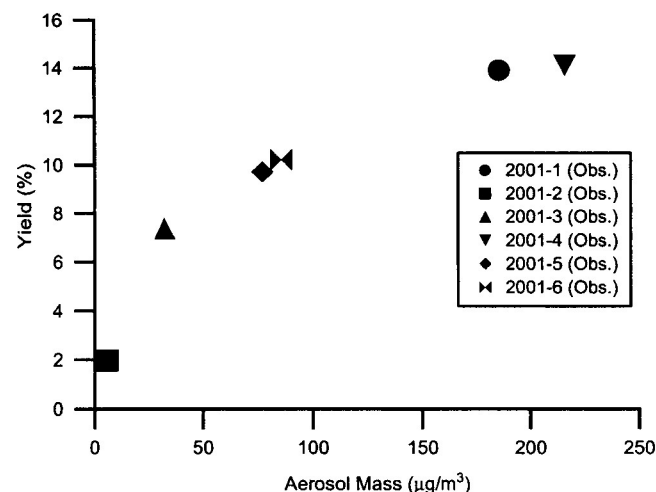


Fig. 1. Yield vs. aerosol mass plot for both observed and modelled experiments for 2001 dataset. Observed values are shown as black symbols, while modelled values are shown as grey symbols.

Table 2

Final conditions for chamber experiments conducted by Barbu (2003). Corrections for dilution and wall loss are incorporated into yield. Isopropyl nitrite was not monitored during experiments.

Experiment date	Toluene (ppmv)	NO (ppmv)	Aerosol yield (%)	Geometric mean (nm)	σ_g
2001-1	0.35	1.71	10	205.19	1.22
2001-2	0.07	0.66	2	86.76	1.46
2001-3	0.12	0.78	7	124.13	1.34
2001-4	0.31	0.88	10	224.62	1.24
2001-5	0.16	1.11	10	157.80	1.30
2001-6	0.16	1.07	10	164.40	1.28

MCM aromatic schemes (Bloss et al., 2005a) as well as with other aromatic chemical mechanisms (Carter, 2007). Metzger et al. (2008), studying 1,3,5 trimethylbenzene, found that the MCMv3.1 shows increased under prediction of reactivity under high NO_x conditions (VOC/NO_x = 0.3), pointing to underestimated sources or overestimated sinks in the radical budget. These weaknesses may contribute to errors in predicted SOA formation in this study.

The model photolysis rates were calculated for summertime, mid-latitude, boundary layer atmospheric conditions and then scaled to match $J(\text{NO}_2) = 2 \times 10^{-3} \text{ s}^{-1}$ determined for the smog chamber at York University (Auld, 2005), to account for the limited spectrum of the chamber lamps. The calculation of photolysis rates is a source of uncertainty due to the difference between the solar spectrum and the black lamp spectrum used in the chamber (Stroud et al., 2004).

An estimated gas-phase wall loss rate of $3 \times 10^{-6} \text{ s}^{-1}$ (Stroud et al., 2004) and a size dependant particle wall loss rate in the range of $(1-2) \times 10^{-5} \text{ s}^{-1}$ (Kelly, 2007; Stroud et al., 2004; Bienenstock, 2001) are used. Preliminary model runs indicated very little sensitivity to the wall loss rates for either the gas or particle phase.

Hynes et al. (2005) suggest an auxiliary mechanism to include in the MCMv3.1 to account for chamber dependant effects: introduction of free radicals through wall reactions, adsorption/desorption of NO_y species on/from the walls and off-gassing of organics from the walls that convert HO to HO₂ and add to ozone production in the system (Bloss et al., 2005a). Here, the reaction rates from the high NO_x limit of Hynes et al. (2005) are included, along with the wall conversion of HONO to NO proposed by Stroud et al. (2004) with a new reaction rate of $1.0 \times 10^{-3} \text{ s}^{-1}$ based on the updated $J(\text{NO}_2)$ value from Auld (2005).

3.2. IPN reduction

Different batches and storage age of the IPN appear to impact its effectiveness as an HO radical source. As the IPN concentration could not be monitored effectively, the initial IPN concentration in the model was scaled by the initial observed loss rate of toluene. This correction ranged from initial ratios of 1/3 to 1/5 for toluene/IPN, compared to the assumed experimental value of 1/10.

3.3. Partitioning theory

The gas-particle partitioning is based on the kinetic theory of Kamens et al. (1999, 2001) where forward and backward rate coefficients are calculated to represent absorption and desorption onto and off of the particles, respectively. The absorptive partitioning is determined by equilibrium constant (iK_p , $\text{m}^3 \mu\text{g}^{-1}$), and the ratio of the rates of absorption (${}^i k_{on}$, $\text{m}^3 \mu\text{g}^{-1} \text{ s}^{-1}$) and desorption (${}^i k_{off}$, s^{-1}).

$${}^iK_p = \frac{{}^i k_{on}}{{}^i k_{off}} \quad (1)$$

For absorption, the equilibrium constant was represented as in Equation (2) (Kamens et al., 1999; Pankow, 1994a,b).

$${}^iK_p = \frac{7.501RTf_{om}}{10^9 MW_{om} \zeta_i {}^i p_L^0} \quad (2)$$

Here, the numerical factors represent appropriate unit conversions, T is the temperature (K), $R = 8.3145 \text{ J mol}^{-1} \text{ K}^{-1}$ is the gas constant, f_{om} is the organic mass fraction (assumed unity, Seinfeld et al., 2001), MW_{om} is the average molecular weight of the absorbing organic material updated according to speciation (g mol^{-1}), ζ_i is the activity coefficient (assumed unity, Stroud et al., 2004) and ${}^i p_L^0$ is the liquid vapour pressure (mmHg). The initial value of MW_{om} is set to the average value of the species proposed to be in the aerosol phase, 180 g mol^{-1} . Experimental vapour pressure data are used when available, but when they are not, they are estimated using Mpbpvp (MPBPWIN v1.41), a freeware estimation program included in EPISUITE (version 3.12) from the Environmental Protection Agency (EPA; EPA, 2007).

In this study, the absorption rate is assumed to be proportional to both the condensing gas and aerosol mass concentrations with a rate constant (${}^i k_{on}$; Stroud et al., 2004) calculated using the uptake coefficient, γ_m (Fuchs and Sutugin, 1970), mean molecular speed, c_i (m s^{-1}), radius, r (m) and particle density, ρ ($\mu\text{g m}^{-3}$).

$${}^i k_{on} = \frac{3\gamma_m c_i}{4r\rho} \quad (3)$$

$$\frac{1}{\gamma_m} = \frac{1}{\alpha} + \frac{3}{4{}^iKn} - \frac{0.47}{1 + {}^iKn} \quad (4)$$

$${}^iKn = \frac{3Dg_i}{c_i r} \quad (5)$$

The accommodation coefficient, α , is set to 0.1, within the range suggested by Jacob (2000), for all species in the base case; the sensitivity to this value will be discussed below. Using the uptake coefficient, shown in Equation (4), allows for the continuum and transition regimes along with the kinetic regime. The Knudsen number, iKn (Seinfeld and Pandis, 1998), is based on the individually estimated diffusion coefficients, Dg_i ($\text{cm}^2 \text{ s}^{-1}$), for each species. The group contribution method of Fuller et al. (Fuller and Giddings, 1965; Fuller et al., 1966, 1969; Reid et al., 1987) is used to estimate the diffusion coefficients, whose values ranged from 0.062 to 0.099 $\text{cm}^2 \text{ s}^{-1}$ over all experiments.

The aerosol size distribution is represented by the geometric mean diameter at each time interval measured, with the assumption that all particles are of uniform size and grow only through condensation. The range in particle size over the course of the experiments is approximately 30–120 nm. However, the size distributions are sufficiently narrow to be represented with a single diameter. Similar to Stroud et al. (2004), sensitivity tests were performed in order to justify the size distribution representation. A constant radius one geometric standard deviation above (and below) the starting geometric mean diameter, capturing the largest (and smallest) particle sizes were used to test the impact of size distribution. A small variation was found in the final aerosol yield ($\pm 15\%$), but fell within estimated experimental error (10–20%).

4. Base case results

The base case results consist of the modelled toluene, NO, and organic aerosol mass, calculated in the box model from the initial experimental conditions and individual IPN correction.

As shown in Figs. 2 and 3, the base case of the model ("EPA" in the figures) generally over-predicts the toluene and NO concentrations after 1 h. The over-predictions in both the toluene and NO could point to problems within the radical budget of the MCMv3.1. The initial agreement between the base case and observations is largely due to the IPN correction, but also includes improvements from the inclusion of the auxiliary mechanism. For experiment 2001–3, toluene has a mean bias (MB) of 2.26×10^{-2} ppm and a mean relative error (MRE) of 17.9%. NO has an MB of 1.69×10^{-1} ppm and an MRE of 22.5%. At the end of the experiment (hour 2–3) the error increases with an MRE of 27.2% and 27.1%, for toluene and NO, respectively. The aerosol yield is largely under predicted with an MB of -6.22% (MRE -83.8%) over the whole experiment and -6.54% (MRE -86.8%) at the end of the experiment. The average HO concentration over the first 30 min is within 10% of the experiment. The average HO concentration is not measured in the chamber but a rough estimate can be derived from the toluene oxidation, assuming it is the most dominant initial reaction for HO. For experiment 2001–6, the agreement values over the whole experiment are: an MB of 5.16×10^{-2} ppb (MRE 30.0%) for toluene, an MB of 1.85×10^{-1} ppm (MRE 18.9%) for NO, an MB of -8.16% (MRE -79.5%) for aerosol yield. The average HO is within 23% of the experiment.

While the model initially captures the features of the toluene and NO decay reasonably well (due to the reduction of initial IPN concentration), it fails to capture the initial onset of aerosol growth and consistently under predicts the overall magnitude of aerosol yield over all the experiments (2001–3 and 2001–6 in Figs. 4 and 5). The under prediction of aerosol mass is partially due to the consistent positive bias in toluene predictions, however, some of the error in the predicted aerosol mass may result from unknown differences inside the chamber not represented in the model (e.g.: additional wall reactions, behaviour of IPN). A series of sensitivity simulations were conducted to determine impacts of different model parameters on aerosol yield.

4.1. Vapour pressure estimation and impact

A similar kinetic partitioning model and chemical mechanism were used by Stroud et al. (2004) to evaluate data from Barbu (2003). Differences between Stroud et al. (2004) and the present work include: the version of the MCM used (3.0 vs. 3.1), the value of $J(\text{NO}_2)$, and the vapour pressure prediction method employed in

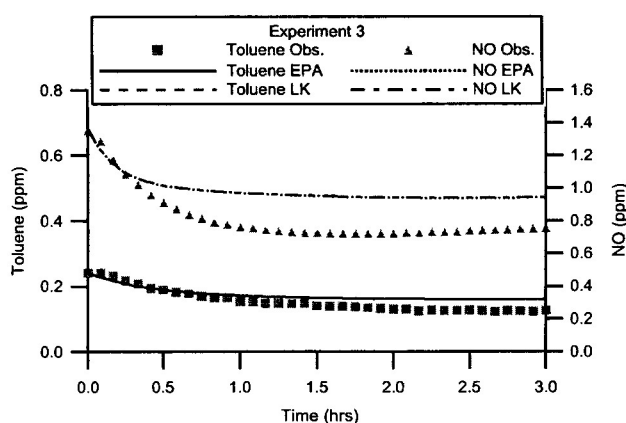


Fig. 2. Toluene and NO results for 2001–3, with vapour pressures estimated using Mpbvvp (EPA) and Lee–Kesler (LK). As expected, different vapour pressure estimation methods have no impact. Observed values are shown as symbols, while modelled values are shown as lines.

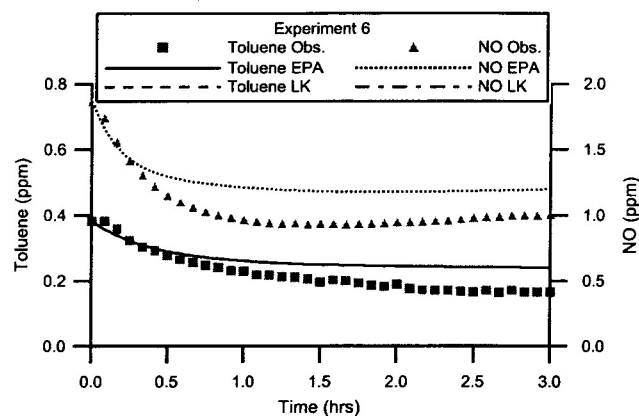


Fig. 3. Toluene and NO results for 2001–6, with vapour pressures estimated using Mpbvvp (EPA) and Lee–Kesler (LK). As expected, different vapour pressure estimation methods have no impact. Observed values are shown as symbols, while modelled values are shown as lines.

the model. Using MCMv3.1 in the present study also impacted the aerosol speciation, due to differences in the branching ratios, reaction rates and chemical species available.

Stroud et al. (2004) used the Lee–Kesler method (Lee and Kesler, 1975; Reid et al., 1987) to predict vapour pressures, with the addition of contribution information for $-\text{ONO}_2$ and $-\text{C}(\text{O})\text{OONO}_2$ groups. This could be one of the main sources of the difference in predicted aerosol mass between their results and the present study. A statistical comparison was performed of predicted vapour pressures from the modified Lee–Kesler and Mpbvvp with the experimental vapour pressures provided by Camredon and Aumont (2006), with the addition of alkyl nitrates and alkyl dinitrates from Capouet and Müller (2006). Due to the large ranges in errors of the predicted values, the natural logarithm of vapour pressure, $\ln(\text{predicted/measured})$, was used as the variable to evaluate the goodness of fit. This metric helps to normalize the impact of over and under prediction by the method in question. Mpbvvp had a smaller mean and root mean square error than Lee–Kesler (0.5 ± 0.7 compared to 0.8 ± 3.0). Mpbvvp performed much better for multi-functional species, alkyl nitrates and alkyl dinitrates.

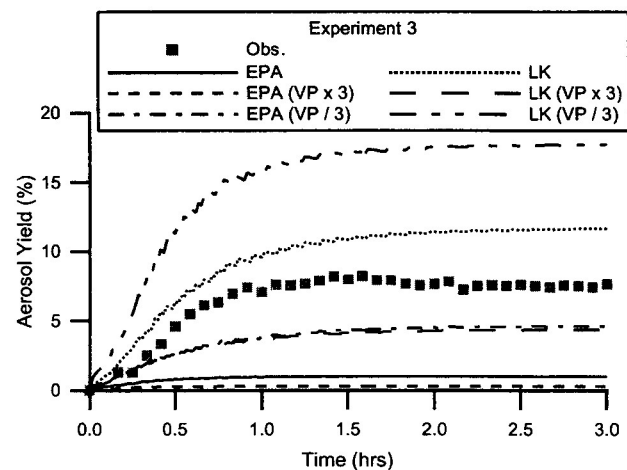


Fig. 4. Aerosol yield prediction results for 2001–3, with vapour pressures estimated using Mpbvvp (EPA) and Lee–Kesler (LK). Observed values are shown as symbols, while modelled values are shown as lines. Vapour pressures are varied by a factor of three to demonstrate impact of the accuracy of vapour pressure estimation method.

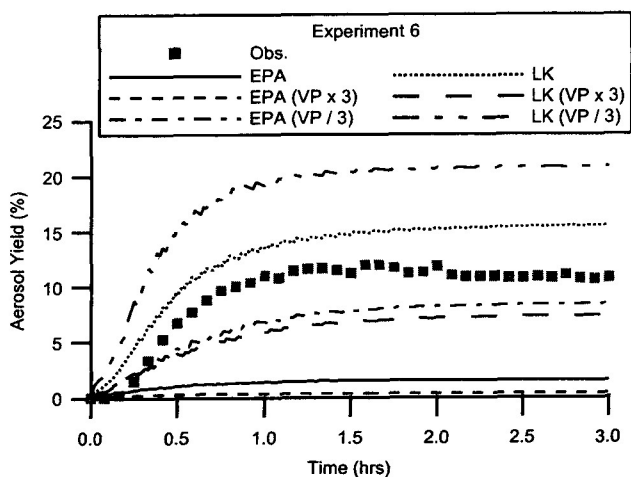


Fig. 5. Aerosol yield prediction results for 2001–6, with vapour pressures estimated using Mpbpvp (EPA) and Lee–Kesler (LK). Observed values are shown as symbols, while modelled values are shown as lines. Vapour pressures are varied by a factor of three to demonstrate impact of the accuracy of vapour pressure estimation method.

Lee–Kesler performed better for PAN species, but only one value was available for comparison. This is likely due to the inclusion of extra groups by Stroud et al. (2004). When applied to the chemical species suggested by MCMv3.1, Lee–Kesler predicted lower vapour pressures, especially for PAN species, than Mpbpvp (top five aerosol species in Table 3, which comprise approximately 99% of the aerosol phase by mass). Mpbpvp does not allow for the introduction of new groups similar to those introduced to Lee–Kesler by Stroud et al. (2004).

When the predicted vapour pressures from Lee–Kesler are used in place of the Mpbpvp values in this study's model, the predicted aerosol yield is observed to increase significantly (Figs. 4 and 5), and reflects the results of Stroud et al. (2004). This illustrates the model's sensitivity to vapour pressures as part of aerosol mass prediction. As seen in Figs. 2 and 3, there is little to no impact on the behaviour of toluene or NO. Most estimation methods can only predict vapour pressures to within a factor of three of the measured value (Camredon and Aumont, 2006; Asher et al., 2002). Hence, it is also important to look at the impact of varying the vapour pressure from each method by a factor of three, highlighting the error range of the model from the vapour pressure alone. For Mpbpvp, increasing the vapour pressure by a factor of three decreased the final aerosol yield by 1.6% on average, over all six experiments. Decreasing the vapour pressures by a factor of three increased the final aerosol yield by 7.0% on average. For Lee–Kesler, increasing the vapour pressure by a factor of three decreased the final yield by 7.0% on average. Decreasing the vapour pressures by a factor of three increased the final aerosol mass by 5.7% on average. The aerosol yield predicted by Mpbpvp when decreased by a factor of three and that predicted by Lee–Kesler when increased by a factor of three are close to one another in all experiments. This indicates the Mpbpvp predicted values would have to decrease by approximately an order of magnitude in order to match the observations. Using either method, it is reasonable to assume an overall range of approximately 10% when looking at the final aerosol yield, but this range varied from 2.8 to 13.5%.

4.2. Accommodation coefficient

The accommodation coefficient impacts the aerosol mass formation through the uptake coefficient in the absorption rate

(Equations (3) and (4)). Varying the accommodation coefficient between 0.1 (base case value) and 0.001 only reduced the aerosol mass, reducing the agreement between model and observations. The accommodation coefficient needs to be sufficiently large such that condensation on the aerosol is faster than condensation on the walls. Given the chamber wall loss rates and the aerosol mass loading for each experiment, the uptake coefficient must be larger than 0.0002. The aerosol is in the kinetic limit, making the uptake coefficient (γ_m) essentially equal to the accommodation coefficient (α). In order to maximize the aerosol mass present in the model with Mpbpvp, larger values of the accommodation coefficient, i.e. unity, could be used. However, whether a value of 0.001, 0.01 or 0.1 is used, the range of predicted aerosol mass still falls within the error range expected from the vapour pressures.

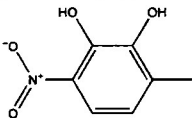
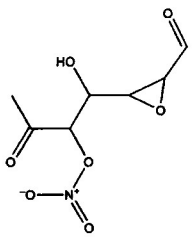
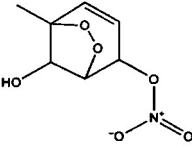
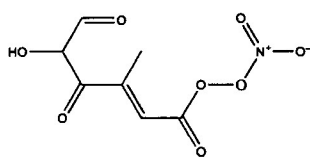
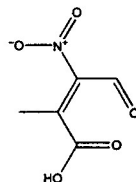
4.3. Aerosol speciation

We used the model to examine the speciation leading to the predictions of aerosol mass. While detailed information is not available for the York chamber, the MCM3.1 speciation used in this study can be compared to other published speciations for toluene oxidation experiments. The species used in the partitioning calculations were selected from the MCM3.1 toluene mechanism based on a ranking of saturation ratios (calculated as the species' partial pressure to vapour pressure ratio) for the top 50 species in the MCMv3.1 for our initial conditions. These preliminary runs do not allow for partitioning between the gas and aerosol phase, therefore the total concentration of the species is in the gas-phase. Only the top 20 species, according to the saturation ratio, are tracked in the model and allowed to partition into the aerosol phase. The model predicted speciation does not vary significantly over the six experiments, with only some changes in order of ranking. Of these top 20 species, five species (Table 3) account for 98% of the aerosol composition by mass, with one species, 3-methyl-6-nitro-catechol ($C_7H_7NO_4$, MNCATECH in MCMv3.1 nomenclature), accounting for nearly 90% of the aerosol mass. In the top five species alone, approximately 10% of the aerosol composition by mass is accounted for by organic nitrates (R–ONO₂).

MNCATECH is predicted by the model to be dominant in both the aerosol and gas-phase, and results from the cresol (C_7H_8O) branch of the toluene reaction mechanism (Fig. 8). The high NO_x conditions in the York chamber (VOC/NO_x = 0.2) are far higher than the high NO_x conditions used to test the MCMv3.1 chemical mechanism (VOC/NO_x = 1.1; Bloss et al., 2005a). The model's prediction of MNCATECH's dominance could be the result of a significant reaction branch, that of cresol formation (R1 in Fig. 8 with a branching ratio of 18%), becoming more dominant and controlling aerosol formation under the chamber's high NO_x conditions (through the reactions directly forming MNCATECH or through differences in the radical budget due to NO_x concentrations). Under the chamber's high NO_x conditions, O₃ formation is suppressed, eliminating R3 and the cycling pathway R6 in Fig. 8. Even under lower NO_x conditions a large concentration of MNCATECH (or subsequent products) is expected as R3 is a much slower reaction than R4. Using the branching ratios of R1 (18%), R2 (73%) and R4 (100%), it can be seen that 13% of toluene goes to the formation of MNCATECH, creating a large gas-phase concentration of MNCATECH (40 times greater) compared to the other species predicted to be in the aerosol phase. This leads to a significantly higher saturation ratio and faster partitioning to the aerosol phase.

The model predicted aerosol speciation is highly dependant on the estimated vapour pressures through the saturation ratio. Given that the accuracy of predicted vapour pressures is expected to be within a factor of three of the true values, errors in the predicted vapour pressures may also affect the speciation. In order to look at

Table 3
 Predicted vapour pressures and structures of the top five aerosol species expected in aerosol phase according to saturation ratio. Relative speciation is for base case scenario.

Species	Vapour pressure (mmHg) and relative speciation (%)		Structure
	Mpbpvp	Lee-Kesler	
MNCATECH	1.79×10^{-5} 89%	2.69×10^{-6} 79%	
TLEMUCNO3	1.19×10^{-5} 6%	2.21×10^{-8} 9%	
TLBIPERNO3	1.28×10^{-4} 3%	2.79×10^{-5} 6%	
C6CO2OHPAN	2.21×10^{-6} 3%	3.23×10^{-10} 2%	
NC4MDCO2H	4.84×10^{-4} 1%	1.31×10^{-5} 3%	

the impact of the vapour pressure of MNCATECH, all other vapour pressures were kept constant while the vapour pressure of MNCATECH was increased by a factor of three and decreased by a factor of three and six (Figs. 6 and 7).

When the vapour pressure of MNCATECH is increased or decreased by a factor of three, the results are very similar to those for when all vapour pressures are increased or decreased. This obviously results from the predicted aerosol mass behaviour being driven by MNCATECH. The speciation remains relatively similar, with a slight increase of 14% from 6% by mass in 1-[(3-formyl-2-hydroxypropyl)oxy]propan-2-yl nitrate ($C_7H_9NO_7$, TLEMUCNO3 in MCMv3.1 nomenclature) for an increase in MNCATECH vapour pressure by a factor of three; this also increases the amount of organic nitrates in the aerosol to 27% from 10%. Not surprisingly, decreasing the vapour pressure of MNCATECH increases its relative importance in the aerosol phase and also increases the total aerosol mass. It was expected that decreasing the vapour pressure of MNCATECH by a factor of six was analogous to decreasing all the vapour pressure by a factor of six. This factor is chosen as the original aerosol mass predictions are at least a factor

of six lower than the observed values. Decreasing the vapour pressures by a factor of six improves the fit of the predicted aerosol mass to the observed, but provides an unrealistic aerosol speciation with MNCATECH contributing 95% of the aerosol by mass.

The model appears to be highly sensitive to changes in MNCATECH. Changing the vapour pressure within the accepted error range largely impacted the aerosol mass prediction but had a much smaller impact on the predicted aerosol speciation. While increasing the vapour pressure of MNCATECH, relative to the other species, would decrease its importance in the aerosol phase, it would also reduce the amount of predicted aerosol mass and increase the relative amount of organic nitrates in the aerosol phase. The use of different vapour pressure estimation methodologies did not affect MNCATECH's dominance of the predicted organic aerosol speciation, and significant sensitivity tests of the MNCATECH vapour pressure similarly had little impact on the model results.

MNCATECH drives the aerosol behaviour through its large gas-phase concentration. In a gas-phase only run (no partitioning) MNCATECH ranks fifth by abundance and has the highest saturation ratio. It is very likely that the high concentration results from

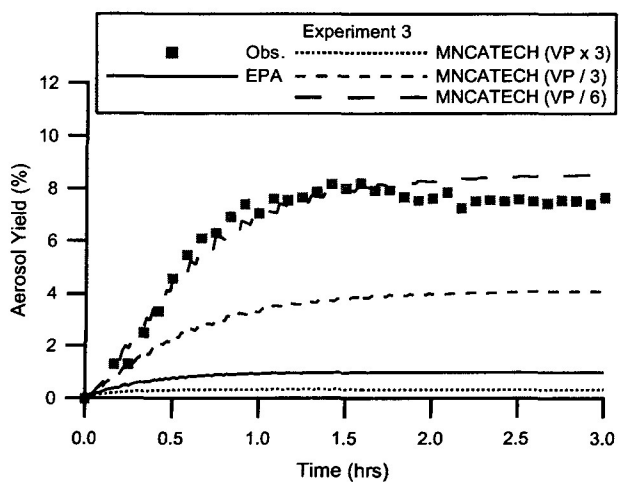


Fig. 6. Aerosol yield prediction results for 2001–3, with vapour pressures varied for aerosol species MNCATECH only, using Mppbvp (EPA). Observed values are shown as symbols, while modelled values are shown as lines.

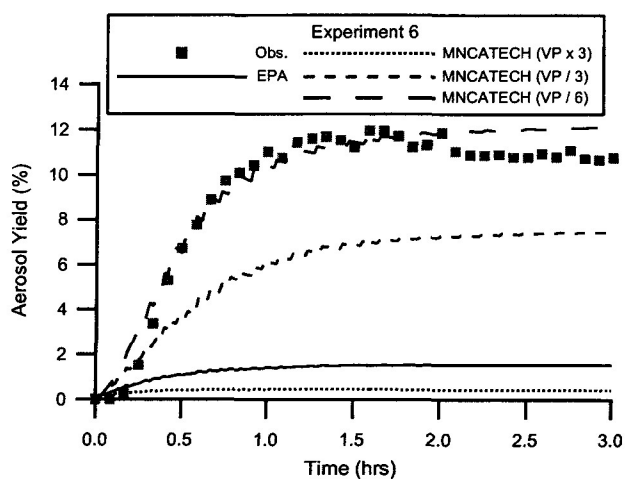


Fig. 7. Aerosol yield prediction results for 2001–6, with vapour pressures varied for aerosol species MNCATECH only, using Mppbvp (EPA). Observed values are shown as symbols, while modelled values are shown as lines.

the high NO_x concentrations in this study. This was determined in sensitivity tests varying the initial VOC/ NO_x ratio. When the amount of NO_x is decreased in the model (VOC/ $\text{NO}_x = 4$, previously 0.2), MNCATECH accounts for approximately 35% of the aerosol phase by mass indirectly through its proposed products, indicating the reaction pathway is of reduced, but still significant, importance for secondary organic aerosol formation. Under high NO_x conditions, VOC oxidation by HO occurs in the presence of competition for the available HO by NO_2 . As the concentration of NO_x decreases relative to VOCs, more HO is available for VOC oxidation and MNCATECH oxidizes further to form its products. Both the high and low NO_x pathways indicate that the MNCATECH formation branches have a significant impact on aerosol formation.

The path of formation and precursor yields to MNCATECH should be investigated in future smog chamber analysis, since the results shown here suggest that it may be an important contributor to aerosol formation, but the a priori testing of the MCMv3.1 for this path did not include high NO_x conditions such as employed here. Recent work with other aromatics in the MCMv3.1 (Metzger et al., 2008) also recommends that more high NO_x evaluation of the mechanism take place.

5. Conclusions

The major objectives in this study were to simulate the observed smog chamber experiments and evaluate the modelled aerosol

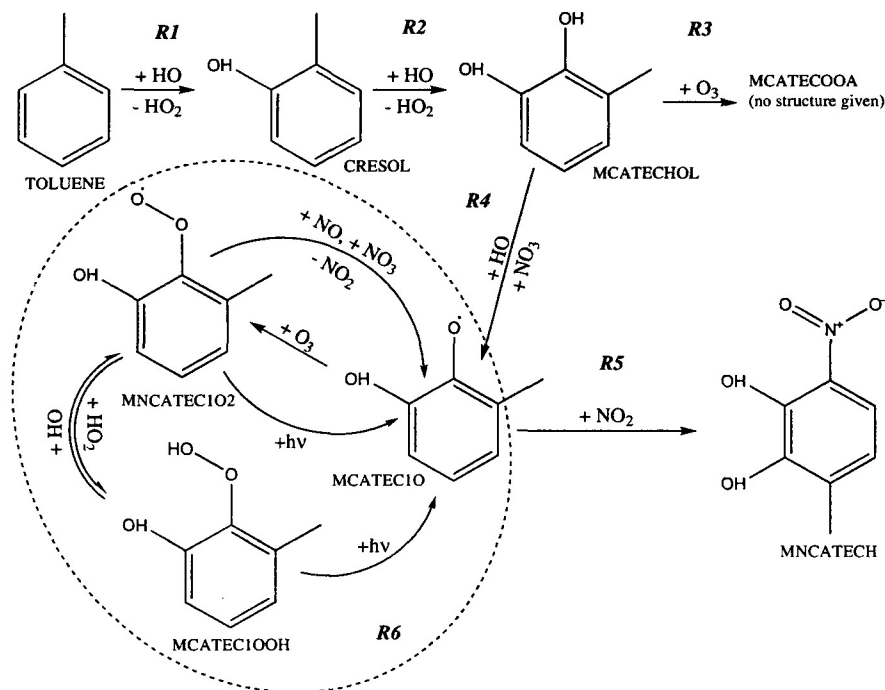


Fig. 8. Proposed reaction mechanism by MCMv3.1 for 3-methyl-6-nitro-catechol (MNCATECH). R1–R6 refer to reaction pathways and MCMv3.1 nomenclature is given for all species. The branching ratios for R1 and R2 are 18% and 73%, respectively.

mass and speciation. Despite the inclusion of the auxiliary mechanism and appropriate IPN corrections, the toluene decay and NO decay fall outside experimental error (10–20%). For the base case, the predicted aerosol yield varies between the six experiments but is largely under predicted for all experiments. In order to understand the aerosol yield prediction further, the factors primary affecting partitioning were examined: vapour pressure and accommodation coefficient. Increasing the vapour pressures by a factor of three decreased the aerosol yield by an average of 1.6% (range of 0.6–2.9%). Decreasing the vapour pressures by a factor of three increased the aerosol yield by an average of 7.0% (range of 2.3–10.7%). Additionally, vapour pressures predicted by the modified Lee–Kesler method of Stroud et al. (2004) were used instead of values predicted by Mpbvpv. As expected, the predicted aerosol yield increased when the lower vapour pressures were used. Increasing these vapour pressures by a factor of three decreased the aerosol yield by an average of 7.0% (range of 5.0–8.1%). Decreasing these vapour pressures by a factor of three increased the aerosol yield by an average of 5.7% (range of 5.3–6.3%). The aerosol mass predicted by the base case (Mpbvpv vapour pressures) was under predicted by at least a factor of six, compared to the observations (yield under predicted by at least a factor of two).

The model is much less sensitive to accommodation coefficient than vapour pressure. Varying the accommodation coefficient by two orders of magnitude resulted in aerosol yield predictions that fell within the lower range of values resulting from the vapour pressure error. A larger value of 0.1, within the suggested range of Jacob (2000), is chosen to maximize the predicted aerosol mass.

The dominance of 3-methyl-6-nitro-catechol (MNCATECH, MCMv3.1 nomenclature) in the aerosol phase is likely a result of the high NO_x conditions used in the chamber. A significant branch in the MCMv3.1 toluene mechanism is taking a more dominant role in SOA formation under higher NO_x conditions than those used to test the mechanism in earlier work. This species comprises approximately 73–88% of the aerosol phase by mass, over the range of accuracy for the vapour pressure (\pm a factor of three), regardless of the prediction method used. Aerosol speciation from the Lee–Kesler method saw slightly higher organic nitrates fractions (\sim 20%) compared to the aerosol speciation from Mpbvpv (\sim 10%). Increases in organic nitrates are coupled with decreases in the relative dominance of MNCATECH.

Sensitivity experiments varying the vapour pressure of MNCATECH relative to other species demonstrated the dominant impact of MNCATECH on the aerosol mass prediction. Whether all the species' vapour pressures, or solely that of MNCATECH, were varied over the range of accuracy, similar results were seen in the predicted aerosol mass. This is most likely due to the large abundance of MNCATECH in the gas-phase, relative to all other species expected to partition in the model (according to saturation ratio).

These results suggest that the toluene oxidation portion of the MCMv3.1 mechanism, specifically the cresol-forming branch, requires further evaluation under high NO_x conditions. The yields of gas-phase cresol and the other products that are precursors to MNCATECH formation may have a significant influence on SOA formation – this needs to be confirmed in laboratory experiments aimed at evaluating these pathways under high NO_x conditions. It is also critical that vapour pressure estimation methods improve for the multi-functional types of species presented here, especially organic nitrates and PAN-type species. This will require more experimentally determined vapour pressures for species that fall under these categories, in order to evaluate the improved estimation methods.

The use of a detailed speciation model has been shown to provide an excellent tool for evaluating a detailed chemical

mechanism and its resulting SOA formation. The model does require evaluation under other chamber conditions, as well as verification of proposed aerosol speciation with measured aerosol products. The use of the model has highlighted a potentially important pathway for organic aerosol formation, while showing the need for gas-phase mechanism evaluation under a high NO_x conditions.

Acknowledgements

This work was supported by the Natural Sciences and Engineering Research Council of Canada (NSERC), the Canadian Foundation for Climate and Atmospheric Sciences (CFCAS) and Environment Canada. The authors would like to acknowledge the passing of their close colleague, Dr. D. V. Michelangeli, and her support and contributions to this project.

References

- Asher, W.E., Pankow, J.F., Erdakos, G.B., Seinfeld, J.H., 2002. Estimating the vapour pressures of multi-functional oxygen-containing organic compounds using group contribution methods. *Atmospheric Environment* 36, 1483–1498.
- Auld, J., 2005. Personal communication.
- Barbu, A.M., 2003. Smog chamber studies of aromatic hydrocarbon photooxidation by hydroxyl radicals. M.Sc. thesis, York University, Toronto, Canada.
- Barsanti, K.C., Pankow, J.F., 2005a. Thermodynamics of the formation of atmospheric organic particulate matter by accretion reactions 1: aldehydes and ketones. *Atmospheric Environment* 38, 4371–4382.
- Barsanti, K.C., Pankow, J.F., 2005b. Thermodynamics of the formation of atmospheric organic particulate matter by accretion reactions 2: dialdehydes, methylglyoxal, and diketones. *Atmospheric Environment* 39, 6597–6607.
- Barsanti, K.C., Pankow, J.F., 2006. Thermodynamics of the formation of atmospheric organic particulate matter by accretion reactions—part 3: carboxylic and dicarboxylic acids. *Atmospheric Environment* 40, 6676–6686.
- Bienestock, Y.S., 2001. Chamber studies of particulate production from hydroxyl reactions with toluene. M.Sc. thesis, York University, Toronto, Canada.
- Bloss, C., Wagner, A., Bonzanini, M.E., Jenkin, K., Wirtz, K., Martin-Reviejo, M., Pilling, M.J., 2005a. Evaluation of detailed aromatic mechanisms (MCMv3 and MCMv3.1) against environmental chamber data. *Atmospheric Chemistry and Physics* 5, 623–639.
- Bloss, C., Wagner, A., Jenkin, K., Volkamer, R., Bloss, W.J., Lee, J.D., Heard, D.E., Wirtz, K., Martin-Reviejo, M., Rea, G., Wenger, J.C., Pilling, M.J., 2005b. Development of a detailed chemical mechanism (MCMv3.1) for the atmospheric oxidation of aromatic hydrocarbons. *Atmospheric Chemistry and Physics* 5, 641–664.
- Camredon, M., Aumont, B., 2006. Assessment of vapour pressure estimation methods for secondary organic aerosol modeling. *Atmospheric Environment* 40, 2105–2116.
- Capouet, M., Müller, J.F., 2006. A group contribution method for estimating the vapour pressures of α -pinene oxidation products. *Atmospheric Chemistry and Physics* 6, 1455–1467.
- Carter, W.P.L., 2007. Conference Summary: International Conference on Atmospheric Chemical Mechanisms. December 6–8, 2006, David, California. URL: http://www.cert.ucr.edu/~carter/Mechanism_Conference/Conference_Summary.pdf.
- Donahue, N.M., Huff Hartz, K.E., Chuong, B., Presto, A.A., Stanier, C.O., Rosenhorn, T., Robinson, A.L., Pandis, S.N., 2005. Critical factors determining the variation in the SOA yields from terpene ozonolysis: a combined experimental and computational study. *Faraday Discussions* 130, 295–309.
- Donahue, N.M., Robinson, A.L., Stanier, C.O., Pandis, S.N., 2006. Coupled partitioning, dilution, and chemical ageing of semivolatile organics. *Environmental Science and Technology* 40, 2635–2643.
- Environmental Protection Agency, 2007. Office of Pollution Prevention and Toxics Exposure Assessment, <http://www.epa.gov/opptintr/exposure/pubs/episuite.htm>.
- Forstner, H.J.L., Flagan, R.C., Seinfeld, J.H., 1997. Secondary organic aerosol from the photooxidation of aromatic hydrocarbons: molecular composition. *Environmental Science and Technology* 31, 1345–1358.
- Fuchs, N.A., Sutugin, A.G., 1970. Highly Dispersed Aerosols. Ann Arbor Science Publishers, Ann Arbor.
- Fuller, E.N., Giddings, J.C., 1965. A comparison of methods for predicting gaseous diffusion coefficients. *Journal of Gas Chromatography* 3, 222–227.
- Fuller, E.N., Schettler, P.D., Giddings, J.C., 1966. New method for prediction of binary gas-phase diffusion coefficients. *Industrial & Engineering Chemistry* 58, 18–27.
- Fuller, E.N., Ensley, K., Giddings, J.C., 1969. Diffusion of halogenated hydrocarbons in helium. The effect of structure on collision cross sections. *Journal of Physical Chemistry* 73, 3679–3685.
- Gery, M.W., Fox, D.L., Jeffries, H.E., Stockburger, L., Weathers, W.S., 1985. A continuous stirred tank reactor investigation of the gas-phase reaction of hydroxyl radicals and toluene. *International Journal of Chemical Kinetics* 17, 931–955.

- Aldebrandt, L., Donahue, N.M., Pandis, S.N., 2009. High formation of secondary organic aerosol from the photo-oxidation of toluene. *Atmospheric Chemistry and Physics Discussions* 9, 693–733.
- Hao, L.Q., Wang, Z.Y., Huang, M.Q., Fang, L., Zhang, W.J., 2007. Effects of seed aerosols on the growth of secondary organic aerosols from the photooxidation of toluene. *Journal of Environmental Sciences* 19, 704–708.
- Hu, D., Kamens, R.M., 2007. Evaluation of the UNC toluene-SOA mechanism with respect to other chamber studies and key model parameters. *Atmospheric Environment* 41, 6465–6477.
- Hu, D., Tolocka, M., Li, Q., Kamens, R.M., 2007. A kinetic mechanism for predicting secondary organic aerosol formation from toluene oxidation in the presence of NO_x and natural sunlight. *Atmospheric Environment* 41, 6478–6496.
- Huang, M.Q., Zhang, W.J., Hao, L.Q., Wang, Z.Y., Zhou, L.Z., Gu, X.J., Fang, L., 2006. Chemical composition and reaction mechanisms for secondary organic aerosol from photooxidation of toluene. *Journal of the Chinese Chemical Society* 53, 1149–1156.
- Hurley, M.D., Sokolov, O., Wallington, T.J., Takekawa, H., Karasawa, M., Klotz, B., Barnes, I., Becker, K.H., 2001. Organic aerosol formation during the atmospheric degradation of toluene. *Environmental Science and Technology* 35, 1358–1366.
- Hynes, R.G., Angove, D.E., Saunders, S.M., Harverd, V., Azzi, M., 2005. Evaluation of two MCMv3.1 alkene mechanisms using indoor environmental chamber data. *Atmospheric Environment* 39, 7251–7262.
- Izumi, K., Fukuyama, T., 1990. Photochemical aerosol formation from aromatic hydrocarbons in the presence of NO_x. *Atmospheric Environment* 24A, 1433–1441.
- Jacob, D.J., 2000. Heterogeneous chemistry and the tropospheric ozone. *Atmospheric Environment* 34, 2131–2159.
- Jang, M., Kamens, R.M., 2001. Characterization of secondary aerosol from the photooxidation of toluene in the presence of NO_x and 1-propene. *Environmental Science and Technology* 35, 3626–3639.
- Jang, M., Czoschke, N.M., Northcross, A.L., Cao, G., Shaof, D., 2006. SOA formation from partitioning and heterogeneous reactions: model study in the presence of inorganic species. *Environmental Science and Technology* 40, 3013–3022.
- Jiang, W.M., 2003. Instantaneous secondary organic aerosol yields and their comparison with overall aerosol yields for aromatic and biogenic hydrocarbons. *Atmospheric Environment* 37, 5439–5444.
- Jeffries, H.E., 1995. Photochemical air pollution. In: Singh, H.B. (Ed.), *Composition, Chemistry, and Climate of the Atmosphere*. Van Nostrand Reinhold, New York.
- Johnson, D., Jenkin, M.E., Wirtz, K., Martin-Reviejo, M., 2004. Simulating the formation of secondary organic aerosol from the photooxidation of toluene. *Environmental Chemistry* 2, 150–165.
- Kamens, R., Jang, M., Chien, C.J., Leach, K., 1999. Aerosol formation from the reaction of α -pinene and ozone using a gas-phase kinetics-aerosol partitioning model. *Environmental Science and Technology* 33, 1430–1438.
- Kamens, R., Jaoui, M., 2001. Modeling aerosol formation from α -pinene + NO_x in the presence of natural sunlight using gas-phase kinetics and gas-particle partitioning theory. *Environmental Science and Technology* 35, 1394–1405.
- Kanakidou, M., Seinfeld, J.H., Pandis, S.N., Barnes, I., Dentener, F.J., Facchini, M.C., Van Dingenen, R., Ervens, B., Nenes, A., Nielsen, C.J., Swietlicki, E., Putaud, J.P., Balkanski, Y., Fuzzi, S., Horth, J., Moortgat, G.K., Winterhalter, R., Myhre, C.E.L., Tsigaridis, K., Vignati, E., Stephanou, E.G., Wilson, J., 2005. Organic aerosol and global climate modelling: a review. *Atmospheric Chemistry and Physics* 5, 1053–1123.
- Kelly, J., 2007. Impact of parameter representation in gas-particle partitioning on aerosol yield model prediction. Ph.D. thesis. York University, Toronto, Canada.
- Kleindienst, T.E., Smith, D.F., Li, W., Edney, E.O., Driscoll, D.J., Speer, R.E., Weathers, W.S., 1999. Secondary organic aerosol formation from the oxidation of toluene. *Atmospheric Environment* 33, 3669–3681.
- Lee, D.I., Kesler, M.G., 1975. A generalized thermodynamic correlation based on three-parameter corresponding states. *American Institute of Chemical Engineers Journal* 21, 510–527.
- Metzger, A., Dommen, J., Gaeggeler, K., Duplissy, J., Prevot, A.S.H., Kleffmann, J., Elshorbary, Y., Wisthaler, A., Baltensperger, U., 2008. Evaluation of 1,3,5-trimethylbenzene degradation in the detailed tropospheric chemistry mechanism, MCMv3.1, using environmental chamber data. *Atmospheric Chemistry and Physics* 8, 6453–6468.
- Ng, N.L., Kroll, J.H., Chan, A.W.H., Chhabra, P.S., Flagan, R.C., Seinfeld, J.H., 2007. Secondary organic aerosol formation from m-xylene, toluene, and benzene. *Atmospheric Chemistry and Physics* 7, 3909–3922.
- Odum, J.R., Jungkamp, P.W., Griffin, R.J., Forstner, H.J.L., Flagan, R.C., Seinfeld, J.H., 1997. Aromatics, reformulated gasoline, and atmospheric organic aerosol formation. *Environmental Science and Technology* 31, 1890–1897.
- Pankow, J.F., 1994a. An absorption model of the gas/aerosol partitioning involved in the formation of secondary organic aerosol. *Atmospheric Environment* 28, 189–193.
- Pankow, J.F., 1994b. An absorption model of gas/particle partitioning of organic compounds in the atmosphere. *Atmospheric Environment* 28, 185–188.
- Pitz, M., Cyrys, J., Karg, E., Wiedensohler, A., Wichmann, H.E., Heinrich, J., 2003. Variability of apparent particle density of an urban aerosol. *Environmental Science and Technology* 37, 4336–4342.
- Presto, A.A., Huff Hartz, K.E., Donahue, N.M., 2005. Secondary organic aerosol production from terpene ozonolysis 2: effect of NO_x concentration. *Environmental Science and Technology* 39, 7046–7054.
- Reid, R.C., Prausnitz, J.M., Poling, B.E., 1987. *The Properties of Gases & Liquids*, fourth ed. McGraw-Hill, Boston.
- Sato, K., Klotz, B., Hatakeyama, S., Imamura, T., Washizu, Y., Matsumi, Y., Washida, N., 2004. Secondary organic aerosol formation during the photooxidation of toluene: dependence on initial hydrocarbon concentration. *Bulletin of the Chemical Society of Japan* 77, 667–671.
- Sato, K., Hatakeyama, S., Imamura, T., 2007. Secondary organic aerosol formation during the photooxidation of toluene: NO_x dependence of chemical composition. *Journal of Physical Chemistry A* 111, 9796–9808.
- Seinfeld, J.H., Erdakos, G.B., Asher, W.E., Pankow, J.F., 2001. Modeling the formation of secondary organic aerosol (SOA) 2. The predicted effects of relative humidity on aerosol formation in the α -pinene/, β -Pinene/, sabinene/, Δ^3 -carene/, and cyclohexene–ozone systems. *Environmental Science and Technology* 35, 1806–1817.
- Seinfeld, J.H., Pandis, S.N., 1998. *Atmospheric Chemistry and Physics: from Air Pollution to Climate Change*. John Wiley & Sons, Inc, New York.
- Song, C., Na, K., Cocker III, D.R., 2005. Impact of the hydrocarbon to NO_x ratio on the secondary organic aerosol formation. *Environmental Science and Technology* 39, 3143–3149.
- Stroud, C.A., Makar, P.A., Michelangeli, D.V., Mozurkewich, M., Hastie, D.R., Barbu, A., Humble, J., 2004. Simulating organic aerosol formation during the photooxidation of toluene/NO_x mixtures: comparing the equilibrium and kinetic assumption. *Environmental Science and Technology* 38, 1471–1479.
- Turpin, B.J., Huntzicker, J.J., 1995. Identification of secondary organic aerosol episodes and quantization of primary and secondary organic aerosol concentrations during SCAQS. *Atmospheric Environment* 29, 3527–3544.
- Xia, A.G., Michelangeli, D.V., Makar, P.A., 2008. Box model studies of the secondary organic aerosol formation under different HC/NO_x conditions using the subset of the Master Chemical Mechanism for α -pinene. *Journal of Geophysical Research* 113, D10301. doi:10.1029/2007JD008726.